Supporting Information

High-Performance Moisture Sensor based on Ultralarge Graphene Oxide

Boon-Hong Wee,[a] Wai-Hwa Khoh,[a] Ashis K. Sarker,[b] Chang-Hee Lee,[b] and Jong-Dal Hong[a]*

[a] Department of Chemistry, Research Institute of Natural Sciences, Incheon National University, 119 Academy-ro, Yeonsu-gu, Incheon, 406-772, Republic of Korea.

[b] Department of Electrical and Computer Engineering, Seoul National University, Seoul 151-742, Republic of Korea

To whom all correspondence should be addressed.

E-mail: hong5506@inu.ac.kr
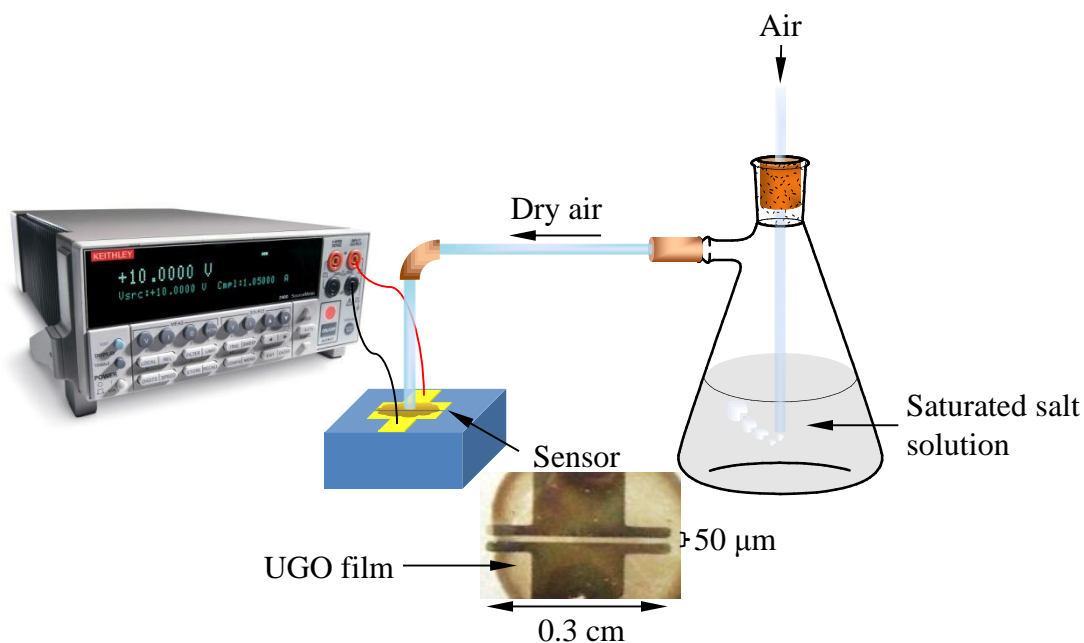
Figure S1. Setup for the dynamic measurement of the humidity sensing properties of UGO and SGO sensor. The length of the gold electrode and inter-electrode gap were fixed at 0.3 cm and 50 μm, respectively.
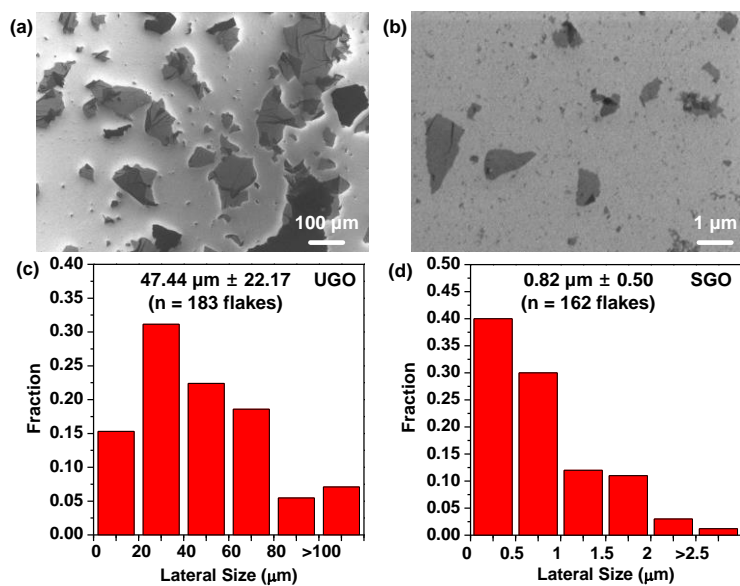
Figure S2. FE-SEM images and histograms for the lateral size distribution of UGO sheets (a,c) and SGO sheets (b,d). Reprinted with permission from Lee, M.; Wee, B. H.; Hong, J. D., *Adv. Energy Mater*. 2015, **5**, DOI: 10.1002/aenm.201401890.[1]
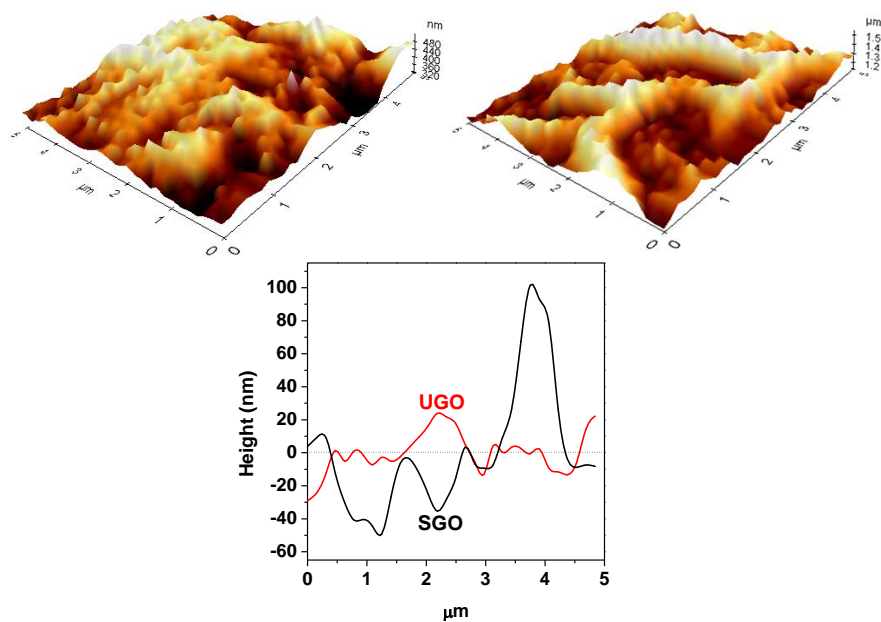
Figure S3. AFM tapping mode images of UGO (top left image) and SGO (top right image), and their corresponding height profile measurements.
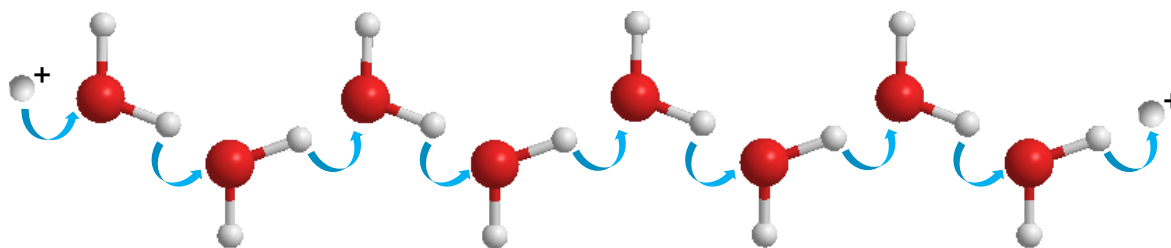
Figure S4 (a) Grotthuss mechanism for proton conduction.

Gold electrode UGO Gold electrode Gold electrode SGO Gold electrode

Carboxylic acid
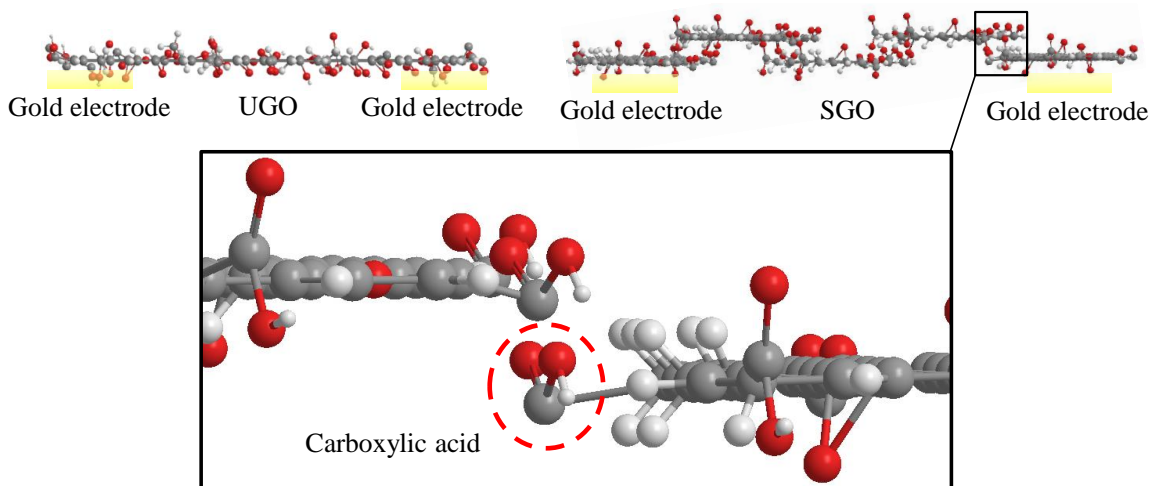
Figure S4. (b) Graphical images of UGO (top left image) and SGO (top right image) films drop-coated onto a pair of gold electrode. These SGO boundaries or edges act as scattering centers that block the proton-transport pathway and thus reducing the overall proton conductivity.

Table S1. Comparison of the high-performance resistive-type humidity sensors

Ref.	Journal	Material	Sensitivity	Relative humidity (Temperature)	Response (Recovery) Time
2	*Adv. Mater.* **2015**	Reduced GO	0.06 (75.7%RH)	4.3-75.7%RH	4 s (10 s)
3	*Nano Lett.* **2013**	Graphene quantum dots	0.5	No data	10 s (20 s)
4	*Adv. Mater.* **2012**	VS_2 ultrathin nanosheets	30 (0-100%RH)	0-100%RH (25 ºC)	30 s (12 s)
5	*J. Phys. Chem. C* **2012**	Carbon nanotube	3.6 (10-70%RH)	10-90%RH (25 ºC)	6 s (120 s)
6	*J. Exp. Nanosci.* **2009**	H-doped Graphene	0.8 (4-84%RH)	4-84%RH (25 ºC)	3 min (few hours)
7	*JACS* **2007**	SnO_2 NW	326 (5-85%RH)	5-85%RH (30 ºC)	120 s (20 s)
8	*Sensor Actuat. B-Chem* **2004**	Nanostructured carbon film	No Data	5-85%RH (20 ºC)	No Data
9	*Phys. Status Solidi A.* **2004**	WO_3/Y_2O_3	1535 (5-98%RH)	5-98%RH (25 ºC)	120 s (360 s)

10	*Cryst. Res. Technol.* **2004**	MgCu Ferrite	No Data	11-100%RH	50 s
11	*Phys. Status Solidi A* **2002**	ZnO-Y$_2$O$_3$	2800 (5-98%RH)	5-98%RH (25 ºC)	No Data
Present study		UGO	4339 (7-100%RH)	7-100%RH (20 ºC)	0.2 s (0.7 s)
Present study		SGO	1982 (7-100%RH)	7-100%RH (20 ºC)	0.1 s (0.3 s)

Spectroscopic Characterizations of UGO and SGO. Surface chemical analysis of the UGO and SGO was performed using X-ray photoelectron spectroscopy (XPS). XPS survey scan of the UGO and SGO films showed two distinct peaks corresponding to C 1s (287.2 eV) and O 1s (534.8 eV), as shown in Figure S5a. The high-resolution XPS spectra of GOs show several relatively well-resolved peaks corresponding to carbon atoms in different chemical environments. The chemical states of C 1s as well as their corresponding area compositions were obtained by peak fitting the respective high energy XPS signal, as shown in Figure S5b, c and Table S2. Interestingly, the peak at 284.5eV corresponding to the aromatic carbon atoms was found to be absent in both UGO and SGO. Similar observation was reported by Kim *et al.*[12] and Szabó *et al.*[13] indicating the loss of aromaticity in fully oxidized GO. The carbon/oxygen (C/O) ratio is a useful parameter for investigating the degree of oxidation of GO.[14] The C/O value for UGO (0.85) was found to be slightly higher than that of SGO (0.75). The C 1s peak of GO can be deconvoluted into four different chemically shifted components namely sp^3 C–C (286.3 eV); C–O (287.3eV); C=O (289.2eV); and C(=O)-(OH) (290.3eV), which agreed well with those reported in the literature.[13, 15, 16] The C–O bonding is attributed to alcohol, phenols, and ethers groups in the basal plane. The C=O bonding mainly originated from single ketones and quinones, which decorate the edges of GO sheets; whereas the C(=O)-(OH) species are present mainly at the edges of GO sheets.[13, 14] Based on the XPS results (Table S2), two very important conclusions can be made that will give valuable insight in explaining the superior performance of UGO as proton conductor. Firstly, the area percentage for C-O in UGO (41.08%) was found to be higher than that in SGO (33.58%). According to Hatakeyama *et al.*, these C-O moieties in the basal plane can provide an important pathway for proton conduction.[17] Secondly, the area percentage for C(=O)-(OH) (6.06 %) in UGO was found to be lower than that in SGO (10.14 %), thereby supporting the fact that smaller SGO sheet has relatively higher amount of edge sites. These edge-to-edge junctions in a SGO film are undesirable in that additional energy is required for proton to hop from one sheet to the neighboring sheet, which can result in blocking the transport of protons.
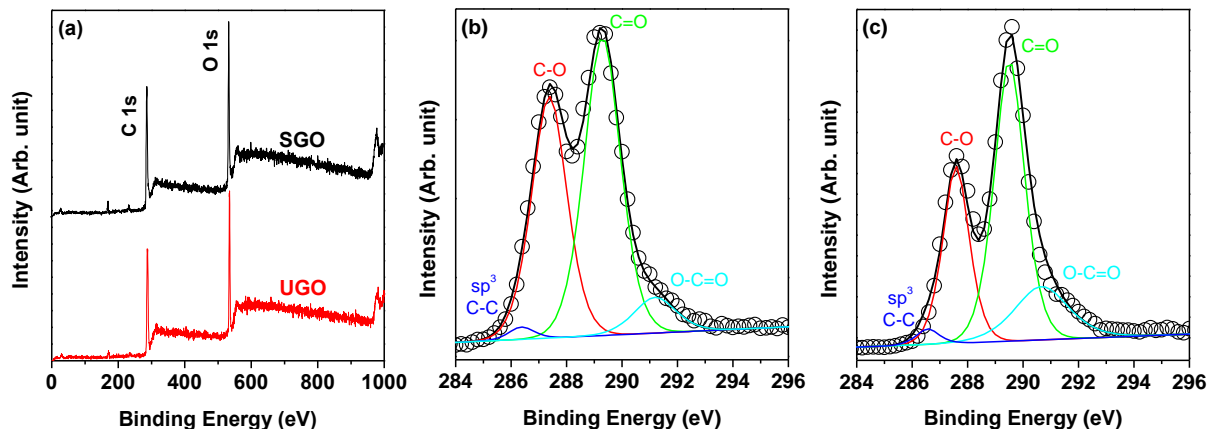
Figure S5. (a) Survey scan and high resolution XPS scan for C 1s for (b) UGO and (c) SGO. (○) in (b) and (c) represents experimental XPS curve, whereas (─) represents the fitted XPS curve by using Gaussian-Lorentzian function after performing a Shirley background correction.

Table S2. The binding energies (eV) and the corresponding area compositions (%) of the chemical states of C 1s core-level peaks in the high energy resolution XPS spectrum of the UGO and SGO thin films

Sample	sp^3 C–C (eV)	C–O (eV)	C=O (eV)	C(=O)-(OH) (eV)	C/O
UGO	2.1 (286.4)	41.1 (287.4)	50.8 (289.4)	6.1 (291.0)	0.85
SGO	2.9 (286.6)	33.6 (287.6)	53.4 (289.5)	10.1 (290.7)	0.75

Raman spectroscopy is a powerful tool to characterize the density of defects in graphene oxide that is considered to be proportional to the oxidation degree of GO.[18] For humidity sensing application, these defects originated from the oxygenated functional groups are essential for governing the proton conducting properties in GO.[18] The D peak at ~ 1350 cm^{-1} is due to the breathing modes of six-atom rings, which is activated due to structural defects. The high degree of disorders in GO was also manifested in the presence of D' peak (~ 1615 cm^{-1}) that overlapped with G peak (~ 1590 cm^{-1}), resulting in a single upshifted broad peak at ~ 1600 cm^{-1}. Therefore, it is more convenient to consider these two overlapping peaks as a single broad peak.[18] The Raman spectra of fully oxidized UGO and SGO can be deconvoluted into 5 peaks, as shown in Figure S6. The average distance between defects (L_D) is proportional to the D-to-G intensity ratio (I_D/I_G) as shown by the relation, $I_D/I_G = $ C'(λ)L_D^2. From the calculation (Table S3), the L_D value for both UGO (1.78 nm) and SGO (1.73 nm) are quite similar, indicating the high degree of structural defects on the basal plane of fully oxidized UGO and SGO.[18] The large value of the full width at half height of G peak (FWHM(G)) also indicated the high structural disorder in UGO and SGO.[19]
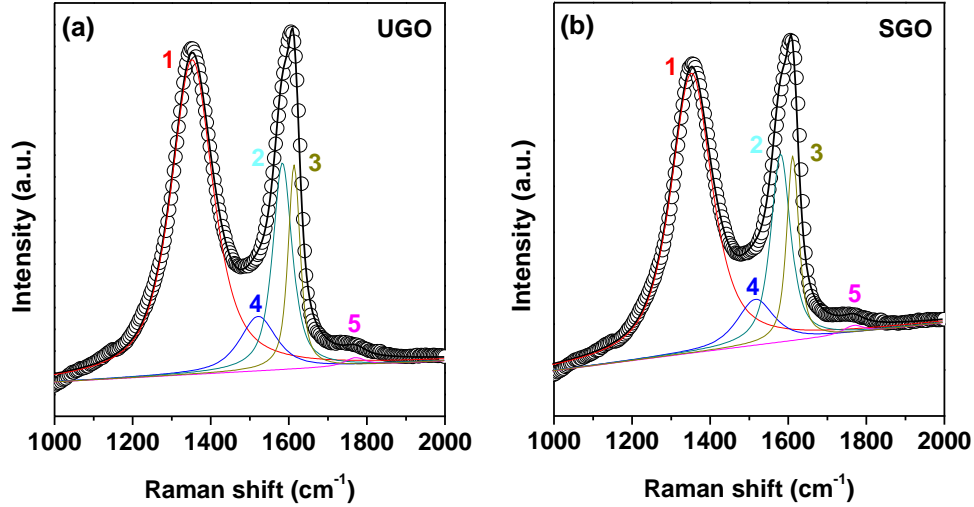
Figure S6. Comparison of the visible Raman spectra (λ_{ex} = 532 nm) of (a) UGO and (b) SGO. (○) represents the experimental Raman spectra, whereas (─) represents the fitted Raman curve by using Gaussian-Lorentzian function. The chemical components used for fitting are shown in curves (1 to 5), where peak 1 is assigned as the D band, peak 2 as G band, peak 3 as D' band, peak 4 as anti-Stokes, and peak 5 as Stokes combination of the E_{2g} LO phonon and the B_{2g} ZO' phonon (layer-breathing mode).[18]

Table S3. D-to-G ratio (I_D/I_G), average distance between defects (L_D) and full width at half height of G peak (FWHM(G)) of UGO and SGO

Sample	I_D/I_G	L_D (nm)	FWHM(G)
UGO	1.98 ±0.01	1.78 ± 0.01	77.8 ±0.4
SGO	1.88 ±0.02	1.73 ± 0.02	79.4 ±0.1

Experimental

Preparation of graphene oxide from thermally expanded graphite. Detailed synthesis procedure can be found in our previous publication.[1] In brief, natural graphite flake (2 g) and conc. H_2SO_4 (60 mL) were stirred rigorously for 24 h. Fuming HNO_3 (20 mL) was added into the mixture while continued stirring for 24 h (room temperature). DI water (80 mL) was added slowly and stirred for another 1 h. After the mixture was washed with DI water (washing step was repeated for three times), it was centrifuged at 4 000 rpm for 20 min, and then the sediment was collected and dried at 60 ^{o}C for 2 days to obtain the graphite intercalation compound (GIC). This compound was placed in a ceramic boat and then inserted into a long quartz tube. The sealed tube was purged with argon (3 cycles of purge and vacuum). In order to obtain the expanded graphite (EG) compound, the sealed quartz tube was inserted slowly into a quartz tube

furnace pre-heated to 1000 ^{o}C. Within 30 sec, the physical appearance of the dense graphite flakes changed drastically to highly expanded graphite powder. In order to synthesize GO from EG, EG powder (1 g) was stirred in 200 mL of conc. H_2SO_4 and then $KMnO_4$ (10 g) was added slowly and stirred for 24 h. After that, DI water (200 mL) and H_2O_2 (50 mL, 35 %) were added slowly into the mixture and stirred for another 30 min. The color of the suspension changed from dark green to light brown. This suspension was repeatedly washed with 10 % HCl (v/v) solution by centrifuging it for three times at 4 000 rpm for 20 min. After that, it was washed with DI water until the pH of the suspension reached 5 to 6.

References

1. M. Lee, B.-H. Wee and J.-D. Hong, *Adv. Energy Mater.*, 2015, **5**, DOI: 10.1002/aenm.201401890.
2. X. Wang, Z. Xiong, Z. Liu and T. Zhang, *Adv. Mater.*, 2015, **27**, 1370-1375.
3. T. S. Sreeprasad, A. A. Rodriguez, J. Colston, A. Graham, E. Shishkin, V. Pallem and V. Berry, *Nano Lett.*, 2013, **13**, 1757-1763.
4. J. Feng, L. Peng, C. Wu, X. Sun, S. Hu, C. Lin, J. Dai, J. Yang and Y. Xie, *Adv. Mater.*, 2012, **24**, 1969-1974.
5. J.-W. Han, B. Kim, J. Li and M. Meyyappan, *J. Phys. Chem. C*, 2012, **116**, 22094-22097.
6. A. Ghosh, D. J. Late, L. S. Panchakarla, A. Govindaraj and C. N. R. Rao, *J. Exp. Nanosci.*, 2009, **4**, 313-322.
7. Q. Kuang, C. Lao, Z. L. Wang, Z. Xie and L. Zheng, *J. Am. Chem. Soc.*, 2007, **129**, 6070-6071.
8. M. Bruzzi, S. Miglio, M. Scaringella, G. Bongiorno, P. Piseri, A. Podesta' and P. Milani, *Sensor Actuat. B-Chem.*, 2004, **100**, 173-176.
9. R. Sundaram and K. S. Nagaraja, *Phys. Status Solidi A*, 2004, **201**, 529-535.
10. N. Rezlescu, E. Rezlescu, C. L. Sava, F. Tudorache and P. D. Popa, *Cryst. Res. Technol.*, 2004, **39**, 548-557.
11. A. M. Edwin Suresh Raj, C. Maria Magdalane and K. S. Nagaraja, *Phys. Status Solidi A*, 2002, **191**, 230-234.
12. J. Jia, C.-M. Kan, X. Lin, X. Shen and J.-K. Kim, *Carbon*, 2014, **77**, 244-254.
13. T. Szabó, O. Berkesi, P. Forgó, K. Josepovits, Y. Sanakis, D. Petridis and I. Dékány, *Chem. Mater.*, 2006, **18**, 2740-2749.
14. X. Lin, X. Shen, Q. Zheng, N. Yousefi, L. Ye, Y.-W. Mai and J.-K. Kim, *ACS Nano*, 2012, **6**, 10708-10719.
15. B.-H. Wee and J.-D. Hong, *Adv. Funct. Mater.*, 2013, **23**, 4657-4666.
16. C. Mattevi, G. Eda, S. Agnoli, S. Miller, K. A. Mkhoyan, O. Celik, D. Mastrogiovanni, G. Granozzi, E. Garfunkel and M. Chhowalla, *Adv. Funct. Mater.*, 2009, **19**, 2577-2583.
17. K. Hatakeyama, M. R. Karim, C. Ogata, H. Tateishi, A. Funatsu, T. Taniguchi, M. Koinuma, S. Hayami and Y. Matsumoto, *Angew. Chem. Int. Edit.*, 2014, **53**, 6997-7000.
18. A. C. Ferrari and D. M. Basko, *Nat. Nanotechnol.*, 2013, **8**, 235-246.

19.   L. G. Cançado, A. Jorio, E. H. M. Ferreira, F. Stavale, C. A. Achete, R. B. Capaz, M. V. O. Moutinho, A. Lombardo, T. S. Kulmala and A. C. Ferrari, *Nano Lett.*, 2011, **11**, 3190-3196.